LLM-RG4: Flexible and Factual Radiology Report Generation across Diverse Input Contexts

Zhuhao Wang[1], Yihua Sun[1], Zihan Li[1], Xuan Yang[1], Fang Chen[2,3], Hongen Liao[1,2,3*]

[1]School of Biomedical Engineering, Tsinghua University, Beijing, China
[2]School of Biomedical Engineering, and [3]Institute of Medical Robotics, Shanghai Jiao Tong University, Shanghai, China
wangzhuh23@mails.tsinghua.edu.cn, liao@tsinghua.edu.cn

Abstract

Drafting radiology reports is a complex task requiring flexibility, where radiologists tail content to available information and particular clinical demands. However, most current radiology report generation (RRG) models are constrained to a fixed task paradigm, such as predicting the full "finding" section from a single image, inherently involving a mismatch between inputs and outputs. The trained models lack the flexibility for diverse inputs and could generate harmful, input-agnostic hallucinations. To bridge the gap between current RRG models and the clinical demands in practice, we first develop a data generation pipeline to create a new MIMIC-RG4 dataset, which considers four common radiology report drafting scenarios and has perfectly corresponded input and output. Secondly, we propose a novel large language model (LLM) based RRG framework, namely LLM-RG4, which utilizes LLM's flexible instruction-following capabilities and extensive general knowledge. We further develop an adaptive token fusion module that offers flexibility to handle diverse scenarios with different input combinations, while minimizing the additional computational burden associated with increased input volumes. Besides, we propose a token-level loss weighting strategy to direct the model's attention towards positive and uncertain descriptions. Experimental results demonstrate that LLM-RG4 achieves state-of-the-art performance in both clinical efficiency and natural language generation on the MIMIC-RG4 and MIMIC-CXR datasets. We quantitatively demonstrate that our model has minimal input-agnostic hallucinations, whereas current open-source models commonly suffer from this problem.

Code — https://github.com/zh-Wang-Med/LLM-RG4

Introduction

The automatic generation of textual descriptions for radiographs has the potential to reduce clinicians' workload, enhance the efficiency of image interpretation, and support informed treatment decisions. Numerous works have concentrated on generating the comprehensive findings section of the report from a single radiology image (Li et al. 2018; Chen et al. 2020, 2021; Wang et al. 2022b, 2023b; Yan et al. 2024). However, certain information in the report is uninferable within a single image, resulting in a mismatch between
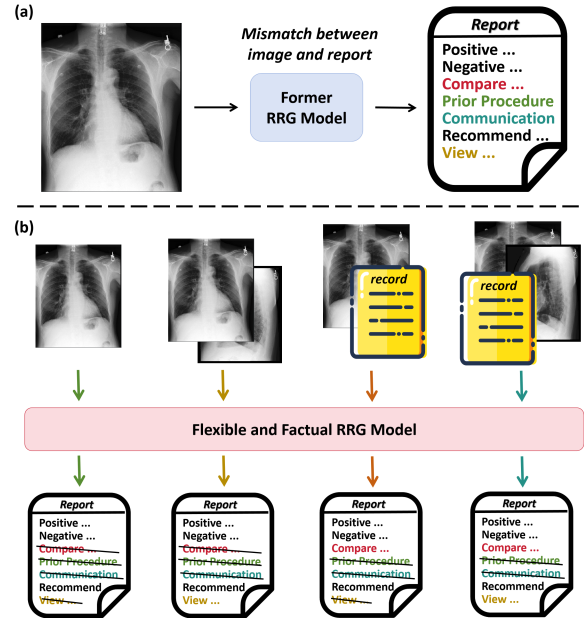
Figure 1: (a) Mismatch between image and report in typical RRG model. Comparisons, procedures, communication and views are uninferable. (b) A flexible and factual RRG paradigm, which emphasizes the flexibility of input and the alignment between input and output.

the input and the output, as illustrated in Figure 1(a). Concretely, Nguyen et al. (2023) classify the information in a report into several key components: positive mentions, negative mentions, prior comparisons, prior procedures, image views, doctor communications, and medical recommendations. Notably, elements such as comparisons, procedures, communication and views are uninferable within a single image. Current paradigm amplifies model hallucination, reduces model performance, and lowers clinical acceptance.

In response to this phenomenon, several studies have sought to clean and reconstruct the report content. For instance, Ramesh, Chi, and Rajpurkar (2022) introduced the GILBERT model, which utilizes token-by-token classification to eliminate comparative descriptions, Thawakar et al. (2024) and Nguyen et al. (2023) leveraged the language

comprehension capabilities of large language models to eliminate uninferable descriptions when provided with a single image. However, such approaches drastically reduce the information included in the report, potentially undermining its effectiveness in fulfilling the intended function of radiology reports (Hartung et al. 2020). Furthermore, several studies have explored multi-view modeling (Yuan et al. 2019; Miura et al. 2021; Lee et al. 2023) and longitudinal historical information modeling (Dalla Serra et al. 2023; Sanjeev et al. 2024) to incorporate addition valid information. However, their performance deteriorates in the absence of additional information, and continues to produce hallucinations

In clinical practice, doctors adaptively draft reports based on available information and clinical requirements (Johnson et al. 2019). The radiologist compare the current findings with previous examinations when historical records are accessible. They integrate information from multiple views if provided, and concentrate on findings within a single frontal view if only one is available. Therefore, a more flexible and factual model for RRG should adapt to diverse input scenarios and produce reports inferred from the input within a unified framework, as illustrated in Figure 1(b). Meanwhile, it is crucial to identify definitive or potential lesions across various input scenarios to ensure timely intervention.

Inspired by clinical practices, this work introduces a flexible and factual framework consisting of a new data generation pipeline and a novel model architecture for RRG. The data generation pipeline produces the MIMIC-RG4 dataset from MIMIC-CXR, taking into account four common input scenarios that involve the integration of multi-view and longitudinal data. The pipeline comprises a BERT-based discriminator, namely DiscBERT, and a generator, Llama3-70B (AI@Meta 2024). It utilizes a cyclic generation approach to ensure that the reconstructed reports closely correspond to the input while minimizing information loss. Additionally, DiscBERT, as a byproduct of the pipeline, allows for quantitative input-agnostic information evaluation. In terms of the model architecture, we introduce LLM-RG4, which utilizes LLM's flexible instruction-following capabilities and extensive general knowledge. (Li et al. 2023a,b; Guo et al. 2023b). To avoid increasing the computational burden with additional input types, we design an adaptive token fusion module that accommodates various inputs while maintaining a consistent token count. The underlying intuition is that an efficient and high-fidelity information encoding for multimodal large language model (MLLM) can be achieved within specialized medical tasks. Furthermore, to improve clinical accuracy, we employ a token-level loss weighting strategy that prioritizes critical diagnoses. This approach enhances clinical efficacy directly at the loss layer, without depending on reinforcement learning (Miura et al. 2021) or classifier-assisted techniques (Jin et al. 2024). We validate our framework through experiments on MIMIC-CXR and MIMIC-RG4. Our contributions are summarized as follows.

- We present a novel paradigm MIMIC-RG4 for pragmatic RRG, introduce a new pipeline for data generation and a product DiscBERT to quantitatively evaluate input-agnostic hallucinations.

- We develop LLM-RG4, a LLM-based RRG model that incorporates an adaptive token fusion module to efficiently accommodate different inputs and a token-level loss weighting strategy to enhance diagnostic accuracy.

- We conduct extensive experiments demonstrating that LLM-RG4 achieves state-of-the-art performance in CE and NLG dimensions on both the MIMIC-CXR and MIMIC-RG4 datasets, while minimizing input-agnostic hallucinations, thus bridging the gap to clinical practice.

MIMIC-RG4 Paradigm

Problem Formulation

In contrast to the typical report generation paradigm, MIMIC-RG4 exhibits two notable differences. Firstly, it requires the model to be able to handle different input scenarios. Secondly, regardless of the input case, the model generates reports corresponding to the inputs.

We define four common clinical input scenarios: single view no longitudinal, multi-view no longitudinal, single view with longitudinal, and multi-view with longitudinal. Longitudinal refers to previous X-ray examinations and here we only include previous reports T_p. Single view refers to frontal image I_f. Multi-view refers to frontal and lateral images I_l. Meanwhile, the indication T_i or history T_h section is also important for report generation (Miura et al. 2021; Hyland et al. 2023), thus we incorporate them as inputs if available. Denote the model as L_g and the current report as T_c, the entire task is formalized as:

$$T_c = L_g(I_f, I_l, T_p, T_h, T_i) \qquad (1)$$

where I_l, T_p, T_i, T_h allow for absence and the corresponding T_c will vary accordingly. With respect to the contents of reports, we follow the definition of Nguyen et al. (2023) and reconstruct the report to maximize the retention of effective information. Specifically, for different input scenarios, the communication and prior procedure are removed. Positive mentions, negative mentions, and medical recommendations are retained. View and prior comparison are retained or rewritten depending on the inputs.

Dataset Generation Pipeline

The overall pipeline is shown in Figure 2. Based on problem formulation, the prior comparison, prior procedure, view, and communication sections are of greater importance. We utilize Llama3-70B model as the generator to reconstruct reports. However, some challenging cases require multiple modifications to meet the requirements. Therefore, we adopt a cyclic process of judgment, rewriting, and re-evaluation until the report is satisfactory. In iterative modifications, the previous process is also used to form a dynamic prompt that fully leverages the model's chain-of-thought (COT) capability. This is a highly time-consuming process. To expedite it, we train a BERT-based model, DiscBERT, as the discriminator to perform judgment tasks. DiscBERT is trained with the Llama3-70B's judgment results, and exhibits judgement capabilities comparable to Llama3-70B. To preserve the diagnostic information of the report, we employ CheXbert to compute the disease labels for the impression section before
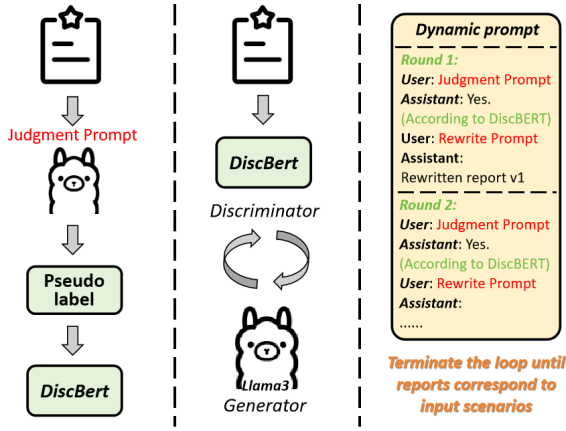
Figure 2: The pipeline employs an iterative approach that integrates a BERT-based discriminator and a LLM-based generator, ensuring minimal input-agnostic information and effective information loss.

Dataset	split	PC(%)	PP(%)	View(%)	Comm(%)
MIMIC CXR	Tr/16.9K	39.90	15.99	1.17	4.56
	Val/0.1K	38.36	11.28	1.50	3.01
	Ts/0.1K	65.63	25.78	3.13	10.16
MIMIC RG4	Tr/172.6K	0.30	0.30	0.12	0.00
	Val/1.4K	0.07	0.07	0.14	0.00
	Ts/2.4K	0.42	0.42	0.04	0.04

Table 1: Percentage of reports with single image no longitudinal setting, that encompass various categories of information. PC: Prior Comparison; PP: Prior Procedure; Comm: Communication; Tr: train; Ts: test.

and after processing. If there is any change in labels, the corresponding example is discarded. We set the maximum iterations to 3 rounds.

Our integrated approach enables us to leverage the COT of LLM while accelerating the pipeline by reducing the reliance on LLM. Moreover, DiscBERT allows for convenient dataset analysis that distinguishes information categories within the generated reports, offering a tool for evaluating input-agnostic hallucinations. Doctors manually label 200 reports to evaluate the discriminatory performance of DiscBERT and assess the effectiveness of the pipeline. The details about DiscBERT, instructions and evaluation are presented in the supplementary material.

Dataset Statistics

We utilize the MIMIC-CXR dataset (Johnson et al. 2019), which is the only publicly available dataset that encompasses both multi-view and longitudinal information, to generate the MIMIC-RG4 dataset. We evaluate the proportion of reports containing input-agnostic information in the MIMIC-CXR and MIMIC-RG4 datasets under the single view no longitudinal setting, as assessed by DiscBERT. As shown in Table 1, a few cases in MIMIC-CXR meet the criterion of single view no longitudinal. However even in these cases, the reports still include a number of descriptions of prior comparisons and procedures. This indicates that obtaining the dataset for single view no longitudinal data directly from MIMIC-CXR is inappropriate. In contrast, MIMIC-RG4 minimizes the presence of input-agnostic information and features a larger dataset scale.

Method

The overall architecture, depicted in Figure 3, consists of three primary components: modality encoder, adaptive token fusion module (ATF), and token-level loss weighting strategy (TLW). The modality encoder utilizes pretrained encoders to extract features from a range of visual and tex-tual inputs. The adaptive token fusion module subsequently compresses and integrates these features into a fixed-length fusion token. This token is then supplied to the LLM alongside instructions and indications/histories for decoding. The token-level loss weighting strategy identifies critical diagnostic tokens and assigns them higher loss weights, thereby directing the model to emphasize positive or ambiguous descriptions regardless of the input conditions.

Modality Encoder

Under different input scenarios, the model can access frontal image I_f, lateral images I_l, and previous examination reports T_p. We utilize frozen image encoder E_v and text encoder E_t to obtain corresponding features v_f, v_l, v_t.

$$v_f = E_v(I_f) \tag{2}$$
$$v_l = E_v(I_l) \tag{3}$$
$$v_t = E_t(T_p) \tag{4}$$

where $v_f, v_l \in \mathbb{R}^{N_I \times D'}, v_t \in \mathbb{R}^{N_T \times D'}$, D' is the dimension of feature obtained from modality encoder, N_I is the number of visual tokens, N_T is the number of text tokens. N_I and N_T are generally distinct, with N_I frequently being larger when higher resolution images are employed.

Adaptive Token Fusion Module

Our objective is to maintain a consistent number of feature tokens across different inputs. For instance, with I_f, I_l and T_p present, we hope to produce a fused feature with dimensions equivalent to those of I_f alone. We first employ perceiver p_f, p_l, p_t (Jaegle et al. 2021) and linear layers to further extract and compress modality feature to a consistent dimension $h_f, h_l, h_t \in \mathbb{R}^{N \times D}$ as follows:

$$h_f = Linear(p_f(v_f, V')) \tag{5}$$
$$h_l = Linear(p_l(v_l, p_f(v_f, V'))) \tag{6}$$
$$h_t = Linear(p_t(v_t, p_f(v_f, V'))) \tag{7}$$

where N is the compressed number of feature tokens and considerably smaller than N_I, D is the feature dimension in LLM. Query tokens in p_f are learnable variables $V' \in \mathbb{R}^{N \times D'}$, whereas the query tokens in p_l, p_t are $p_f(v_f, V'))$ derived from frontal image. This approach leverages the frontal image as the primary feature for modality integration, underscoring its critical role across different scenarios.
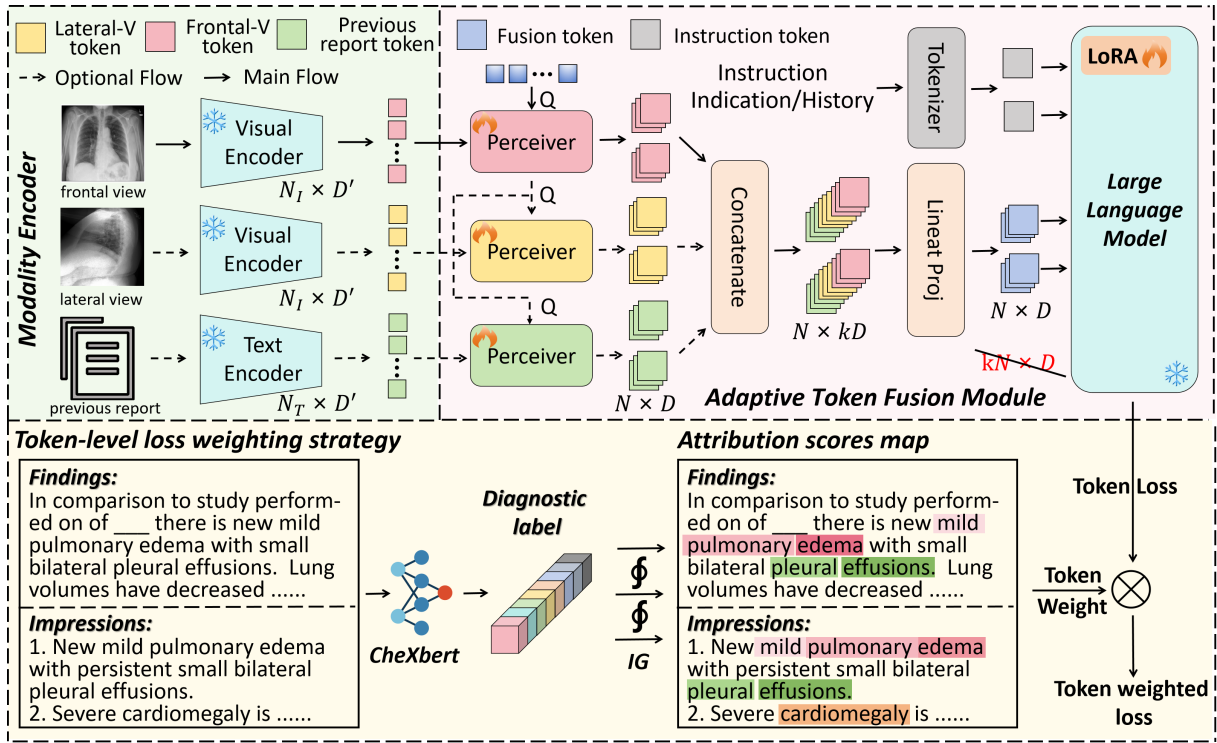
Figure 3: The LLM-RG4 architecture consists of a modality encoder, an adaptive token fusion module, and a token-level loss weighting strategy. The modality encoder extracts features from various modalities. The adaptive token fusion module combines different feature tokens into a fixed length, minimizing computational burden. The token-level loss weighting strategy identifies key diagnoses and adjusts token loss weights, enhancing the model's clinical efficacy across diverse input scenarios.

Typical visual instruction tuning can be viewed as stacking modality features along the token dimension, and escalates computational complexity with increasing input volumes. Given that instruction tuning enables a LLM to understand unseen visual tokens, it is also feasible to train it to comprehend mixed visual-linguistic tokens similarly. Therefore, we consider compressing information along the feature dimensions of each token. Specifically, we first concatenate h_f, h_l, $h_t \in \mathbb{R}^{N \times D}$ along the feature dimensions and get $h_o \in \mathbb{R}^{N \times 3D}$, formulated as:

$$h_0 = concat(h_f, h_l, h_t, dim = 1) \tag{8}$$

If h_l or h_t are not available, we replace it with zeros. To avoid confusion between different modalities, the concatenation order is fixed. A linear projection layer is utilized to maintain the feature dimensions, resulting in the final features h'_o, which are then input into the LLM. This approach guarantees that the number of feature tokens remains constant while efficiently encoding modality information across varying input scenarios.

Token-Level Loss Weighting Strategy

We denote the logit computation function as $f(\theta)$, where θ is the parameter of LLM, denote the current report with a length L as $T = [t^1, t^2, t^3, \ldots, t^L]$, and denote the instruction as P. The predicted logit o is depicted as:

$$o^j = f_\theta(P, h_o, T^{<j}) \tag{9}$$

where $T^{<j}$ represents previous tokens before position j in the current report. The loss at token t^j is depicted as:

$$L_{\text{MLE}}^{(t^j)} = -c_j \log_{\text{softmax}}(o^j) \tag{10}$$

where $c_j = 1$, for $j = 1, 2, \ldots, L$, if all tokens are treated equally. To identify key diagnostic tokens in each report and subsequently adjust the coefficient c_j for each token loss, we utilize CheXbert (Smit et al. 2020) and Integrated Gradients (IG) (Sundararajan, Taly, and Yan 2017). CheXbert conducts multi-label categorization to identify diagnostic labels $Y = [y_1, y_2, y_3, \ldots, y_{14}]$ for 14 distinct diseases in reports. $y_i \in \{-1, 0, 1, 2\}$, -1 indicates uncertainty, 0 indicates negative, 1 indicates positive, 2 indicates not mentioned.

Given that the 14th category in CheXbert is "NO FINDING", we focus solely on the attribution maps of the first 13 categories. The detailed algorithm is depicted in Algorithm 1. We use CheXbert to identify uncertain or positive diagnostic labels in the report and apply Integrated Gradients to generate attribution maps for each label. We then maximize these maps and smooth them with a Gaussian kernel to mitigate token anomaly. If a token's attribution score exceeds a threshold, the weight of each token in the whole sentence is increased to λ. Otherwise, it remains unchanged. Through this approach, we emphasize entire sentences with positive or uncertain diagnoses, minimizing the impact of minor discrepancies between tokens and attribution scores resulting from different tokenizers.

Model	CE Metrics			Clean NLG			Original NLG			*hall.*
	P	R	F1	B@1	B@4	R-L	B@1	B@4	R-L	
R2Gen(Chen et al. 2020)	0.456	0.306	0.366	0.363	0.090	0.269	0.356	0.097	0.267	0.779
R2GenCMN(Chen et al. 2021)	0.486	0.400	0.439	0.385	0.102	0.278	0.349	0.094	0.270	0.695
CVT2Dis.(Nicolson, Dowling, and Koopman 2023a)	0.498	0.414	0.452	0.374	0.103	0.272	0.390	0.123	0.282	0.875
KiUT[†](Huang, Zhang, and Zhang 2023)	0.371	0.318	0.321	-	-	-	0.391	0.113	0.285	-
RGRG[†](Tanida et al. 2023)	0.461	0.475	0.447	-	-	-	0.373	0.126	0.264	-
EKAGen[†](Bu et al. 2024)	0.517	0.483	0.499	-	-	-	0.419	0.117	0.287	-
Promptmrg(Jin et al. 2024)	**0.618**	0.491	0.548	0.326	0.080	0.261	0.381	0.096	0.258	0.896
R2GenGPT(7B)(Wang et al. 2023c)	0.506	0.414	0.456	0.401	0.118	0.277	0.396	0.113	0.273	0.917
CheXagent(7B)(Chen et al. 2024)	0.506	0.306	0.381	0.265	0.058	0.239	0.189	0.040	0.208	0.549
MAIRA-1(7B)[†](Hyland et al. 2023)	-	-	0.553	-	-	-	0.392	0.142	0.289	-
Med-PaLM(562B)[†](Tu et al. 2024)	-	-	0.516	-	-	-	0.317	0.115	0.275	-
R2-LLM(14.2B)[†](Liu et al. 2024a)	0.465	0.482	0.473	-	-	-	0.402	0.128	0.291	-
InVERGe(7B)[†](Deria et al. 2024)	-	-	-	-	-	-	**0.425**	0.100	0.309	-
Ours	0.583	**0.593**	**0.588**	**0.498**	**0.203**	**0.387**	0.377	**0.144**	**0.318**	**0.015**

Table 2: Comparison with SOTA methods for the setting of *sn*. † indicates the results are quoted from the published literature. **Clean NLG** refers to using the cleaned reports from MIMIC-RG4 as ground truth, while **Original NLG** denotes using the original reports from MIMIC-CXR as ground truth. *hall.* means the percentage of reports containing input-agnostic information. The best results are in **bold**.

Experimental Setup

Datasets and Metrics

We train LLM-RG4 on MIMIC-RG4 consisting of four input scenarios: single view no longitudinal, multi-view no longitudinal, single view with longitudinal, and multi-view with longitudinal (denoted as *sn*, *sw*, *mn*, *mw* below). We include the indication/history section as input when available.

Model performance is assessed across three dimensions: natural language generation (NLG), clinical efficacy (CE), and hallucination (*hall.*). For NLG, we use BLEU (B@n) (Papineni et al. 2002), METEOR (MTR) (Banerjee and Lavie 2005) and ROUGE-L (R-L) (Lin 2004). For CE, we adopt CheXbert to extract category labels and calculate

---

Algorithm 1: Detailed Procedure of Token Weight C

Input: Report $T = [t^1, t^2, t^3, \ldots, t^L]$, CheXbert f_c
Output: $C = [c_1, c_2, c_3, \ldots, c_L]$

1: Initialize $c_i = -1$
2: Get $Y = [y_1, y_2, y_3, \ldots, y_{13}] = f_c(T)$
3: **For** y_j **in** G:
4:    **if** $y_j = -1$ or 1: **then**
5:      $c_i' = \text{IG}_i(x)$
6:      $c_i = \max(c_i, c_i')$
7: Define $g_k = \frac{1}{\sqrt{2\pi\sigma^2}} e^{-\frac{k^2}{2\sigma^2}}$
8: Split C into M sentences $C^s = [c^1, c^2, c^3, \ldots, c^M]$, c^n is the nth sentence's weights with length Ln, $c^n = [c_1^n, c_2^n, c_3^n, \ldots, c_{L_n}^n]$.
9: **if** $c_i^n > threshold$ **then**
10:    $c^n = \lambda$ and $\lambda > 1$
11: **else**
12:    $c^n = 1$
13: **end if**
14: **return** C

---

micro-averaged precision (P), recall (R), and F1-score (F1), following established settings (Jin et al. 2024). For hallucinations, we emphasize input-agnostic hallucinations (*hall.*) and employ DiscBERT to measure the proportion of generated reports containing input-agnostic information. A lower value of *hall.* reflects a diminished occurrence of input-agnostic hallucination. Additionally, we use the Wilcoxon Signed-Rank Test (Woolson 2005) to assess performance improvements over baselines. All reports are kept untruncated during testing.

Baselines

Comparative experiments are performed on the traditional *sn* task and the multi-task MIMIC-RG4. For traditional *sn*, we adopt frontal images and focus solely on the findings section in MIMIC-CXR following (Chen et al. 2020). For MIMIC-RG4, both finding and impression are evaluated. We retrain the encoder-decoder model CXRMate (Nicolson, Dowling, and Koopman 2023b), which handles four input scenarios and is trained with reinforcement learning. Additionally, we compare LLM-RG4 with RadFM (Wu et al. 2023), a 14B radiology multimodal large language model capable of processing interleaved text and image inputs.

Implementation Details

We adopt RAD-DINO (Pérez-García et al. 2024) as the image encoder and BiomedVLP-CXRBERT (Boecking et al. 2022) as the text encoder, with Vicuna 7B v1.5 (Chiang et al. 2023) as the text decoder. The number of learnable variable tokens in the perceiver is set to 128, threshold is set to 0.4 and λ is set to 1.75. Following LLAVA (Liu et al. 2024b), we employ a two-stage training strategy. Initially, we only train the ATF with *sn* data to achieve modality alignment. Subsequently, we conduct instruction tuning on the MIMIC-RG4 dataset, training the ATF, and applying LoRA (Hu et al. 2021) for fine-tuning Vicuna.

Dataset	Model	CE Metrics			NLG Metrics ($p < 0.05$)						*hall.*
		P	R	F1	B@1	B@2	B@3	B@4	R-L	MTR	
RG4 *sn*	cxrmate*	$0.572^{\ddagger}$	$0.560^{\ddagger}$	$0.566^{\ddagger}$	$0.421^{\ddagger}$	$0.271^{\ddagger}$	$0.179^{\ddagger}$	$0.122^{\ddagger}$	$0.311^{\ddagger}$	$0.174^{\ddagger}$	**0.010**
	RadFM	$0.413^{\ddagger}$	$0.303^{\ddagger}$	$0.350^{\ddagger}$	$0.188^{\ddagger}$	$0.090^{\ddagger}$	$0.048^{\ddagger}$	$0.028^{\ddagger}$	$0.190^{\ddagger}$	$0.094^{\ddagger}$	$0.737^{\ddagger}$
	Ours	**0.588**	**0.632**	**0.609**	**0.479**	**0.343**	**0.255**	**0.196**	**0.384**	**0.209**	0.014
RG4 *sw*	cxrmate*	$0.573^{\ddagger}$	$0.549^{\ddagger}$	$0.561^{\ddagger}$	$0.361^{\ddagger}$	$0.220^{\ddagger}$	$0.139^{\ddagger}$	$0.093^{\ddagger}$	$0.284^{\ddagger}$	$0.153^{\ddagger}$	**0.009**
	RadFM	$0.508^{\ddagger}$	$0.365^{\ddagger}$	$0.425^{\ddagger}$	$0.211^{\ddagger}$	$0.103^{\ddagger}$	$0.056^{\ddagger}$	$0.033^{\ddagger}$	$0.183^{\ddagger}$	$0.105^{\ddagger}$	$0.092^{\ddagger}$
	Ours	**0.599**	**0.622**	**0.610**	**0.455**	**0.321**	**0.239**	**0.186**	**0.382**	**0.199**	0.021
RG4 *mn*	cxrmate*	**0.544**	$0.522^{\ddagger}$	$0.533^{\ddagger}$	$0.437^{\ddagger}$	$0.289^{\ddagger}$	$0.199^{\ddagger}$	$0.141^{\ddagger}$	$0.332^{\ddagger}$	$0.179^{\ddagger}$	0.009
	RadFM	$0.323^{\ddagger}$	$0.187^{\ddagger}$	$0.237^{\ddagger}$	$0.246^{\ddagger}$	$0.113^{\ddagger}$	$0.060^{\ddagger}$	$0.034^{\ddagger}$	$0.194^{\ddagger}$	$0.104^{\ddagger}$	$0.140^{\ddagger}$
	Ours	0.541	**0.578**	**0.559**	**0.491**	**0.359**	**0.274**	**0.216**	**0.405**	**0.214**	**0.008**
RG4 *mw*	cxrmate*	$0.548^{\ddagger}$	$0.499^{\ddagger}$	$0.523^{\ddagger}$	$0.379^{\ddagger}$	$0.241^{\ddagger}$	$0.158^{\ddagger}$	$0.110^{\ddagger}$	$0.305^{\ddagger}$	$0.159^{\ddagger}$	0.007
	RadFM	$0.456^{\ddagger}$	$0.297^{\ddagger}$	$0.360^{\ddagger}$	$0.191^{\ddagger}$	$0.095^{\ddagger}$	$0.054^{\ddagger}$	$0.034^{\ddagger}$	$0.178^{\ddagger}$	$0.095^{\ddagger}$	$0.052^{\ddagger}$
	Ours	**0.560**	**0.565**	**0.563**	**0.461**	**0.331**	**0.250**	**0.197**	**0.401**	**0.204**	**0.002**

Table 3: Comparison with SOTA methods supporting MIMIC-RG4 across four settings. * indicates the model is retrained on MIMIC-RG4. ‡ denotes statistical significance in paired comparisons with LLM-RG4 based on the Wilcoxon signed-rank test. *hall.* means the percentage of reports containing input-agnostic information. The best results are in **bold**.

Results and Analysis

Overall Results

Table 1 presents the experimental results on the conventional *sn* task. Benefiting from the token-level loss weighting strategy, LLM-RG4 shows a 4.0% and a 3.5% absolute improvement respectively in F1 score over best classifier-assisted model Promptmrg and MAIRA-1 of the same 7B size using 1369 visual tokens. In clean NLG, where ground truth reports get 2.3% *hall.* score, LLM-RG4 has a 24.2% relative improvement in BLEU-4 and a 39.2% relative improvement in ROUGE-L, attributed to training on a cleaner dataset. Regarding hallucination, we find most open-source models suffer from hallucination problems. Even a multi-tasking model CheXagent also gets a 54.9% *hall.* score. However, LLM-RG4 achieves only a 1.5% *hall.* score, indicating that it exhibits minimal input-agnostic hallucinations. Finally, we compute the original-NLG metrics with MIMIC-CXR reports for comparison with powerful closed-source models. Surprisingly, although the ground truth reports attain a 88.5% *hall.* score, our model remains competitive with SOTA models. Both BLEU-4 score and ROUGE-L score of LLM-RG4 are comparable to or slightly exceed the SOTA specialised large multimodal model MAIRA-1. The minimal *hall.* suggests a substantial number of valid descriptions matching the ground truth. This result likely arises from our model being trained on a mixture of four kinds of clean reports, which enhance its learning of valid descriptions.

Under the MIMIC-RG4 setting, LLM-RG4 outperforms all existing models supporting MIMIC-RG4. Although cxrmate utilized reinforcement learning to enhance clinical accuracy, we still achieve an average absolute F1 improvement of 3.8% across four tasks. LLM-RG4's superior performance on NLG metrics further demonstrates that the MLLM architecture is well-suited for multi-tasks featuring flexible language generaion. While RadFM can support interleaved text and image inputs, it performs unsatisfactorily and exhibits a significant input-agnostic hallucination issue on the *sn* setting likely due to overfitting.

Ablation Analysis

We conduct ablation experiments of alternative model designs, as shown in Table 4. The adaptive token fusion module helps reduce feature tokens by approximately 60% when both multi-view and longitudinal information are available, offering similar or slightly better performance than original interleaved inputs. This supports our hypothesis that, efficient and high-fidelity encoding for MLLM can be achieved within specialized medical tasks. TLW benefits CE results on both ATF architecture and interleaved inputs architecture, suggesting that assigning higher loss weights to positive and uncertain descriptions during training can effectively enhance the model's focus on underlying lesions. This phenomenon is evident in both the first and second stages. Further analyses about the ATF module and TLW module are provided in the supplementary materials.

stage	ATF	TLW	N.	F1 Score		NLG	
				F-14	F-5	B@1	B@4
1	-	✗	128	0.519	0.563	0.388	0.126
1	-	✔	128	**0.580**	**0.619**	**0.400**	**0.129**
2	✗	✗	502	0.551	0.582	0.468	0.201
2	✗	✔	502	0.577	0.603	0.469	0.197
2	✔	✗	**204**	0.556	0.580	0.467	**0.205**
2	✔	✔	**204**	**0.585**	**0.610**	**0.472**	0.199

Table 4: Ablation study of each module on MIMIC-RG4. Stage2 results are the average scores across four settings. N. means the max input token numbers.
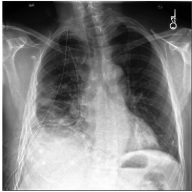
frontal image lateral image	sn (+TLW): *findings : two chest tubes are in place and there is no evidence of pneumothorax . opacification at the right base is prominent consistent with residual pleural fluid and atelectatic changes . subcutaneous emphysema is present along the right lateral chest wall . left lung is essentially clear except for mild atelectatic changes at the base .*
	sw (+TLW): *finding : in comparison with the study of there is little overall change in the appearance of the three right chest tubes with no evidence of pneumothorax . subcutaneous emphysema along the right lateral chest wall appears to be slightly less than on the previous study . opacification at the right base again could reflect post-surgical changes with some atelectatic changes and small effusion . left lung is essentially clear .*
last report: *finding : the patient has undergone vats decortication ....*	mn (+TLW): *finding : there is a small apical pneumothorax on the right with chest tube in place . opacification at the right base is consistent with residual atelectasis and effusion . subcutaneous emphysema is present along the right lateral chest wall extending into the neck . mild atelectatic changes are seen at the left base .*
Gold Standard: *finding : in comparison with the study of there is some decrease in the opacification at the right base . chest tubes remain in place and there is no evidence of pneumothorax . some residual atelectasis and effusion are noted . the possibility of supervening pneumonia at the right base could not be excluded . the left lung is essentially clear with mild atelectatic changes at the base . subcutaneous emphysema persists along the right lateral upper abdominal wall .*	mw (+TLW): *finding : in comparison with the study of there is little overall change in the appearance of the three right chest tubes with no evidence of pneumothorax . subcutaneous emphysema is again seen along the right lateral chest wall . opacification at the right base again could reflect atelectasis and effusion though in the appropriate clinical setting superimposed pneumonia would have to be considered . left lung remains clear .*
	mw (-TLW): *finding : in comparison with the study of there is little change in the appearance of the right hemithorax with three chest tubes in place and no definite pneumothorax . opacification at the right base again is consistent with some combination of atelectasis and re-expansion edema . in the appropriate clinical setting superimposed pneumonia would have to be considered .*

Figure 4: An illustration of a challenging case featuring five positive or uncertain diagnoses across four different settings, where the gold standard is also presented for reference. Diagnosis shared by the gold standard and model outputs are highlighted in the same color. LLM-RG4 identifies nearly all diagnoses, whereas the absence of TLW leads to the missing of two diagnoses.

Influence of Mixed Training

To further investigate whether mixed training across the four settings yields improvement, we train each setting individually for the same number of epochs, shown in Table 5. We find that mixed training lead to varying degrees of improvement across different scenarios, particularly in challenging settings (*mn*, *mw*). We hypothesize that such mixed training can be regarded as a form of data augmentation, effectively increasing the diversity of the training data. It explicitly enables the model to learn the varying demands across different settings during training.

Setting	T.S.	CE Metrics			NLG Metrics		
		P	R	F1	B@1	B@4	R-L
sn	S	**0.589**	0.609	0.599	0.456	0.186	0.384
	M	0.588	**0.632**	**0.609**	**0.479**	**0.196**	**0.384**
sw	S	0.596	0.588	0.592	0.427	0.173	0.376
	M	**0.599**	**0.622**	**0.610**	**0.455**	**0.186**	**0.382**
mn	S	0.526	0.531	0.528	0.464	0.202	0.384
	M	**0.541**	**0.578**	**0.559**	**0.491**	**0.216**	**0.405**
mw	S	0.519	0.544	0.531	0.446	0.179	0.384
	M	**0.560**	**0.565**	**0.563**	**0.461**	**0.197**	**0.401**

Table 5: Influence of mixed training across four settings. T.S. represents the training strategy, **M** represents mixed training, **S** represents training on the specific setting.

Case study

We present a qualitative example to illustrate LLM-RG4's flexibility of diverse inputs and investigate the impact of the TLW module on the model's capabilities, as shown in Figure 3. We select a challenging case involving a patient with confirmed or suspected diagnoses of five different diseases. In the context of multi-view X-ray inputs and longitudinal data, the reports generated by LLM-RG4 accurately cover all five diseases, demonstrating its clinical diagnostic accuracy. In the absence of the token-level loss weighting strategy (TLW), the generated reports lack two diagnostic information. Additionally, the comparative description appears only when longitudinal data is included (*sw*, *mw*), indicating consistency between model inputs and outputs. For the limitations of LLM-RG4, while it provides four types of diagnostic descriptions under scenarios such as *sn*, *sw*, and *mn*, it does not mention the need to consider pneumonia. In the *mn* scenario, it suspects the presence of a small pneumothorax. Future work should further constrain LLM-RG4 to ensure the consistency across different input scenarios. Such enhancement would be beneficial for clinical practice.

Conclusion

In this work, we introduce MIMIC-RG4, a novel paradigm for radiology report generation that adapts to varying input scenarios, aligning more closely with clinical report writing practices. We further propose ATF and TLW to enhance the flexibility and accuracy of large language models in handling diverse inputs, with a consistent emphasis on identifying pathological findings across different settings. Experiments conducted on two datasets illustrate the effectiveness of our method, highlighting that MLLM can achieve more compact information encoding for specific medical tasks. Additionally, the emphasis on key semantic tokens at the loss layer is crucial for enhancing clinical efficacy. We hope these efforts will provide new insights into radiology report generation and the application of large language models in biomedical domains.

References

AI@Meta. 2024. Llama 3 Model Card.

Banerjee, S.; and Lavie, A. 2005. METEOR: An automatic metric for MT evaluation with improved correlation with human judgments. In *Proceedings of the acl workshop on intrinsic and extrinsic evaluation measures for machine translation and/or summarization*, 65–72.

Boecking, B.; Usuyama, N.; Bannur, S.; Castro, D. C.; Schwaighofer, A.; Hyland, S.; Wetscherek, M.; Naumann, T.; Nori, A.; Alvarez-Valle, J.; et al. 2022. Making the most of text semantics to improve biomedical vision–language processing. In *European conference on computer vision*, 1–21. Springer.

Bu, S.; Li, T.; Yang, Y.; and Dai, Z. 2024. Instance-level Expert Knowledge and Aggregate Discriminative Attention for Radiology Report Generation. In *Proceedings of the IEEE/CVF Conference on Computer Vision and Pattern Recognition*, 14194–14204.

Chen, Z.; Shen, Y.; Song, Y.; and Wan, X. 2021. Cross-modal Memory Networks for Radiology Report Generation. In *Proceedings of the 59th Annual Meeting of the Association for Computational Linguistics and the 11th International Joint Conference on Natural Language Processing (Volume 1: Long Papers)*, 5904–5914.

Chen, Z.; Song, Y.; Chang, T.-H.; and Wan, X. 2020. Generating Radiology Reports via Memory-driven Transformer. In *Proceedings of the 2020 Conference on Empirical Methods in Natural Language Processing (EMNLP)*, 1439–1449.

Chen, Z.; Varma, M.; Delbrouck, J.-B.; Paschali, M.; Blankemeier, L.; Van Veen, D.; Valanarasu, J. M. J.; Youssef, A.; Cohen, J. P.; Reis, E. P.; et al. 2024. Chexagent: Towards a foundation model for chest x-ray interpretation. *arXiv preprint arXiv:2401.12208*.

Chiang, W.-L.; Li, Z.; Lin, Z.; Sheng, Y.; Wu, Z.; Zhang, H.; Zheng, L.; Zhuang, S.; Zhuang, Y.; Gonzalez, J. E.; et al. 2023. Vicuna: An open-source chatbot impressing gpt-4 with 90%* chatgpt quality. *See https://vicuna. lmsys. org (accessed 14 April 2023)*, 2(3): 6.

Dalla Serra, F.; Wang, C.; Deligianni, F.; Dalton, J.; and O'Neil, A. 2023. Controllable Chest X-Ray Report Generation from Longitudinal Representations. In *Findings of the Association for Computational Linguistics: EMNLP 2023*, 4891–4904.

Deria, A.; Kumar, K.; Chakraborty, S.; Mahapatra, D.; and Roy, S. 2024. InVERGe: Intelligent Visual Encoder for Bridging Modalities in Report Generation. In *Proceedings of the IEEE/CVF Conference on Computer Vision and Pattern Recognition*, 2028–2038.

Devlin, J. 2018. Bert: Pre-training of deep bidirectional transformers for language understanding. *arXiv preprint arXiv:1810.04805*.

Guo, Z.; Tang, Y.; Zhang, R.; Wang, D.; Wang, Z.; Zhao, B.; and Li, X. 2023a. Viewrefer: Grasp the multi-view knowledge for 3d visual grounding. In *Proceedings of the IEEE/CVF International Conference on Computer Vision*, 15372–15383.

Guo, Z.; Zhang, R.; Zhu, X.; Tang, Y.; Ma, X.; Han, J.; Chen, K.; Gao, P.; Li, X.; Li, H.; et al. 2023b. Point-bind & point-llm: Aligning point cloud with multi-modality for 3d understanding, generation, and instruction following. *arXiv preprint arXiv:2309.00615*.

Hartung, M. P.; Bickle, I. C.; Gaillard, F.; and Kanne, J. P. 2020. How to create a great radiology report. *Radiographics*, 40(6): 1658–1670.

Hu, E. J.; Shen, Y.; Wallis, P.; Allen-Zhu, Z.; Li, Y.; Wang, S.; Wang, L.; and Chen, W. 2021. Lora: Low-rank adaptation of large language models. *arXiv preprint arXiv:2106.09685*.

Huang, Z.; Zhang, X.; and Zhang, S. 2023. Kiut: Knowledge-injected u-transformer for radiology report generation. In *Proceedings of the IEEE/CVF Conference on Computer Vision and Pattern Recognition*, 19809–19818.

Hyland, S. L.; Bannur, S.; Bouzid, K.; Castro, D. C.; Ranjit, M.; Schwaighofer, A.; Pérez-García, F.; Salvatelli, V.; Srivastav, S.; Thieme, A.; et al. 2023. Maira-1: A specialised large multimodal model for radiology report generation. *arXiv preprint arXiv:2311.13668*.

Jaegle, A.; Gimeno, F.; Brock, A.; Vinyals, O.; Zisserman, A.; and Carreira, J. 2021. Perceiver: General perception with iterative attention. In *International conference on machine learning*, 4651–4664. PMLR.

Jin, H.; Che, H.; Lin, Y.; and Chen, H. 2024. Promptmrg: Diagnosis-driven prompts for medical report generation. In *Proceedings of the AAAI Conference on Artificial Intelligence*, volume 38, 2607–2615.

Johnson, A. E.; Pollard, T. J.; Berkowitz, S. J.; Greenbaum, N. R.; Lungren, M. P.; Deng, C.-y.; Mark, R. G.; and Horng, S. 2019. MIMIC-CXR, a de-identified publicly available database of chest radiographs with free-text reports. *Scientific data*, 6(1): 317.

Lee, H.; Kim, W.; Kim, J.-H.; Kim, T.; Kim, J.; Sunwoo, L.; and Choi, E. 2023. Unified chest x-ray and radiology report generation model with multi-view chest x-rays. *arXiv preprint arXiv:2302.12172*, 3(7): 8.

Li, B.; Zhang, Y.; Chen, L.; Wang, J.; Pu, F.; Yang, J.; Li, C.; and Liu, Z. 2023a. Mimic-it: Multi-modal in-context instruction tuning. *arXiv preprint arXiv:2306.05425*.

Li, J.; Li, D.; Savarese, S.; and Hoi, S. 2023b. BLIP-2: bootstrapping language-image pre-training with frozen image encoders and large language models. In *Proceedings of the 40th International Conference on Machine Learning*, 19730–19742.

Li, M.; Lin, B.; Chen, Z.; Lin, H.; Liang, X.; and Chang, X. 2023c. Dynamic graph enhanced contrastive learning for chest x-ray report generation. In *Proceedings of the IEEE/CVF Conference on Computer Vision and Pattern Recognition*, 3334–3343.

Li, Y.; Liang, X.; Hu, Z.; and Xing, E. P. 2018. Hybrid retrieval-generation reinforced agent for medical image report generation. *Advances in neural information processing systems*, 31.

Lin, C.-Y. 2004. Rouge: A package for automatic evaluation of summaries. In *Text summarization branches out*, 74–81.

Lin, Z.; Gou, Z.; Gong, Y.; Liu, X.; Shen, Y.; Xu, R.; Lin, C.; Yang, Y.; Jiao, J.; Duan, N.; et al. 2024. Rho-1: Not all tokens are what you need. *arXiv preprint arXiv:2404.07965*.

Liu, C.; Tian, Y.; Chen, W.; Song, Y.; and Zhang, Y. 2024a. Bootstrapping Large Language Models for Radiology Report Generation. In *Proceedings of the AAAI Conference on Artificial Intelligence*, volume 38, 18635–18643.

Liu, H.; Li, C.; Wu, Q.; and Lee, Y. J. 2024b. Visual instruction tuning. *Advances in neural information processing systems*, 36.

Miura, Y.; Zhang, Y.; Tsai, E.; Langlotz, C.; and Jurafsky, D. 2021. Improving Factual Completeness and Consistency of Image-to-Text Radiology Report Generation. In *Proceedings of the 2021 Conference of the North American Chapter of the Association for Computational Linguistics: Human Language Technologies*, 5288–5304.

Nguyen, D.; Chen, C.; He, H.; and Tan, C. 2023. Pragmatic radiology report generation. In *Machine Learning for Health (ML4H)*, 385–402. PMLR.

Nguyen, H. T.; Nie, D.; Badamdorj, T.; Liu, Y.; Zhu, Y.; Truong, J.; and Cheng, L. 2021. Automated generation of accurate\& fluent medical x-ray reports. *arXiv preprint arXiv:2108.12126*.

Nicolson, A.; Dowling, J.; and Koopman, B. 2023a. Improving chest X-ray report generation by leveraging warm starting. *Artificial intelligence in medicine*, 144: 102633.

Nicolson, A.; Dowling, J.; and Koopman, B. 2023b. Longitudinal Data and a Semantic Similarity Reward for Chest X-Ray Report Generation. *arXiv preprint arXiv:2307.09758*.

Papineni, K.; Roukos, S.; Ward, T.; and Zhu, W.-J. 2002. Bleu: a method for automatic evaluation of machine translation. In *Proceedings of the 40th annual meeting of the Association for Computational Linguistics*, 311–318.

Pérez-García, F.; Sharma, H.; Bond-Taylor, S.; Bouzid, K.; Salvatelli, V.; Ilse, M.; Bannur, S.; Castro, D. C.; Schwaighofer, A.; Lungren, M. P.; et al. 2024. RAD-DINO: Exploring Scalable Medical Image Encoders Beyond Text Supervision. *arXiv preprint arXiv:2401.10815*.

Ramesh, V.; Chi, N. A.; and Rajpurkar, P. 2022. Improving radiology report generation systems by removing hallucinated references to non-existent priors. In *Machine Learning for Health*, 456–473. PMLR.

Sanjeev, S.; Maani, F. A.; Abzhanov, A.; Papineni, V. R.; Almakky, I.; Papież, B. W.; and Yaqub, M. 2024. TiBiX: Leveraging Temporal Information for Bidirectional X-ray and Report Generation. *arXiv preprint arXiv:2403.13343*.

Serra, F. D.; Wang, C.; Deligianni, F.; Dalton, J.; and O'Neil, A. Q. 2023. Controllable chest x-ray report generation from longitudinal representations. *arXiv preprint arXiv:2310.05881*.

Smit, A.; Jain, S.; Rajpurkar, P.; Pareek, A.; Ng, A. Y.; and Lungren, M. 2020. Combining Automatic Labelers and Expert Annotations for Accurate Radiology Report Labeling Using BERT. In *Proceedings of the 2020 Conference on Empirical Methods in Natural Language Processing (EMNLP)*, 1500–1519.

Sun, Y.; Khor, H. G.; Wang, Y.; Wang, Z.; Zhao, H.; Zhang, Y.; Ma, L.; Zheng, Z.; and Liao, H. 2024. Continually Tuning a Large Language Model for Multi-domain Radiology Report Generation. In *International Conference on Medical Image Computing and Computer-Assisted Intervention*, 177–187. Springer.

Sundararajan, M.; Taly, A.; and Yan, Q. 2017. Axiomatic attribution for deep networks. In *International conference on machine learning*, 3319–3328. PMLR.

Tang, Y.; Zhang, R.; Guo, Z.; Ma, X.; Zhao, B.; Wang, Z.; Wang, D.; and Li, X. 2024. Point-PEFT: Parameter-efficient fine-tuning for 3D pre-trained models. In *Proceedings of the AAAI Conference on Artificial Intelligence*, volume 38, 5171–5179.

Tanida, T.; Müller, P.; Kaissis, G.; and Rueckert, D. 2023. Interactive and explainable region-guided radiology report generation. In *Proceedings of the IEEE/CVF Conference on Computer Vision and Pattern Recognition*, 7433–7442.

Thawakar, O. C.; Shaker, A. M.; Mullappilly, S. S.; Cholakkal, H.; Anwer, R. M.; Khan, S.; Laaksonen, J.; and Khan, F. 2024. XrayGPT: Chest Radiographs Summarization using Large Medical Vision-Language Models. In *Proceedings of the 23rd Workshop on Biomedical Natural Language Processing*, 440–448.

Tu, T.; Azizi, S.; Driess, D.; Schaekermann, M.; Amin, M.; Chang, P.-C.; Carroll, A.; Lau, C.; Tanno, R.; Ktena, I.; et al. 2024. Towards generalist biomedical AI. *NEJM AI*, 1(3): AIoa2300138.

Wang, J.; Bhalerao, A.; and He, Y. 2022. Cross-modal prototype driven network for radiology report generation. In *European Conference on Computer Vision*, 563–579. Springer.

Wang, S.; Zhao, Z.; Ouyang, X.; Wang, Q.; and Shen, D. 2023a. ChatCAD: interactive computer-aided diagnosis on medical image using large language models. arXiv. doi: 10.48550. *arXiv preprint arXiv.2302.07257*.

Wang, Z.; Han, H.; Wang, L.; Li, X.; and Zhou, L. 2022a. Automated radiographic report generation purely on transformer: A multicriteria supervised approach. *IEEE Transactions on Medical Imaging*, 41(10): 2803–2813.

Wang, Z.; Liu, L.; Wang, L.; and Zhou, L. 2023b. Metransformer: Radiology report generation by transformer with multiple learnable expert tokens. In *Proceedings of the IEEE/CVF Conference on Computer Vision and Pattern Recognition*, 11558–11567.

Wang, Z.; Liu, L.; Wang, L.; and Zhou, L. 2023c. R2gengpt: Radiology report generation with frozen llms. *Meta-Radiology*, 1(3): 100033.

Wang, Z.; Tang, M.; Wang, L.; Li, X.; and Zhou, L. 2022b. A medical semantic-assisted transformer for radiographic report generation. In *International Conference on Medical Image Computing and Computer-Assisted Intervention*, 655–664. Springer.

Woolson, R. F. 2005. Wilcoxon signed-rank test. *Encyclopedia of Biostatistics*, 8.

Wu, C.; Zhang, X.; Zhang, Y.; Wang, Y.; and Xie, W. 2023. Towards generalist foundation model for radiology. *arXiv preprint arXiv:2308.02463*.

Wu, Y.; Huang, I.-C.; and Huang, X. 2023. Token Imbalance Adaptation for Radiology Report Generation. In *Conference on Health, Inference, and Learning*, 72–85. PMLR.

Xiao, X.; Wu, B.; Wang, J.; Li, C.; Zhou, X.; and Guo, H. 2024. Seeing the Image: Prioritizing Visual Correlation by Contrastive Alignment. *arXiv preprint arXiv:2405.17871*.

Yan, A.; He, Z.; Lu, X.; Du, J.; Chang, E.; Gentili, A.; McAuley, J.; and Hsu, C.-N. 2021. Weakly supervised contrastive learning for chest x-ray report generation. *arXiv preprint arXiv:2109.12242*.

Yan, S.; Cheung, W. K.; Tsang, I. W.; Chiu, K.; Tong, T. M.; Cheung, K. C.; and See, S. 2024. AHIVE: Anatomy-aware Hierarchical Vision Encoding for Interactive Radiology Report Retrieval. In *Proceedings of the IEEE/CVF Conference on Computer Vision and Pattern Recognition*, 14324–14333.

Yuan, J.; Liao, H.; Luo, R.; and Luo, J. 2019. Automatic radiology report generation based on multi-view image fusion and medical concept enrichment. In *Medical Image Computing and Computer Assisted Intervention–MICCAI 2019: 22nd International Conference, Shenzhen, China, October 13–17, 2019, Proceedings, Part VI 22*, 721–729. Springer.

Zhang, Y.; Wang, X.; Xu, Z.; Yu, Q.; Yuille, A.; and Xu, D. 2020. When radiology report generation meets knowledge graph. In *Proceedings of the AAAI conference on artificial intelligence*, volume 34, 12910–12917.

Zhao, Z.; Wang, S.; Gu, J.; Zhu, Y.; Mei, L.; Zhuang, Z.; Cui, Z.; Wang, Q.; and Shen, D. 2024. Chatcad+: Towards a universal and reliable interactive cad using llms. *IEEE Transactions on Medical Imaging*.

Appendix

Related Works

Different Paradigm in CXR   CXR report generation tasks typically produce the findings section from a single image, treating lateral views as independent samples (Chen et al. 2020, 2021). These tasks often employ encoder-decoder architectures that follow the image captioning paradigm and improve generated reports by optimizing network structures (Wang, Bhalerao, and He 2022; Wang et al. 2023b; Huang, Zhang, and Zhang 2023; Yan et al. 2021) or incorporating external prior information (Zhang et al. 2020; Li et al. 2023c). Nguyen et al. (2021) investigated the impact of different view scans and histories on report generation. Serra et al. (2023) modeled longitudinal historical information, introducing a framework to align, concatenate, and fuse current and prior scans into a joint representation. Sanjeev et al. (2024) and Lee et al. (2023) attempted to merge report and image generation within a unified framework. Our paradigm focuses on clinical practice and emphasizes the flexibility and realism of report generation. It requires a unified model that generate various, factual reports across real-world scenarios (w or w/o multi-view, w or w/o longitudinal data) for the same patient.

Large Language Model for Report Generation   The advent of large-scale language models has significantly advanced the field of visual language (Liu et al. 2024b; Li et al. 2023b; Guo et al. 2023a; Tang et al. 2024). Numerous studies have leveraged these models for radiology report generation. Compared to training models from scratch on small datasets, using a large language model as a text decoder effectively utilizes its pretrained capabilities on large-scale datasets. Wang et al. (2023a); Zhao et al. (2024) translated results from computer-aided diagnosis networks into linguistic form, enabling integration of outputs from various networks. Wang et al. (2023c) and Thawakar et al. (2024) adopted visual tuning instructions, freezing large language models, and fine-tuning image encoders or connectors. Liu et al. (2024a) proposed bootstrapping LLMs for RRG with in-domain instance induction and a coarse-to-fine decoding process. Deria et al. (2024) presented a Cross-Modal Query Fusion Layer to enhance alignment between vision and language. Hyland et al. (2023) explored key components affecting model performance, such as domain-specific image encoders, data augmentation, and the indications section. Sun et al. (2024) proposed a continual learning approach tailored for report generation to address the challenge of catastrophic forgetting. Current large model-based report generation generally follows the format of visual instruction tuning. However, this format increases the token number with more inputs, leading to a greater computational burden. Our adaptive token fusion addresses this by using the visual token of the current main view as a query, interacting with other information to obtain fusion feature. This approach ensures that the different information interacts with each other and does not generate additional tokens. Reports can also be generated directly using the main view visual token when no other information is available.

Token-level Loss Weighting Strategy   Each term in a radiology report carries a distinct level of significance and should not be treated uniformly. Wang et al. (2022a) utilized the TF-IDF metric to measure the frequency of occurrence of each word and assigned different weights. Wu, Huang, and Huang (2023) penalized frequently generated tokens while using reinforcement learning to constantly update the range of frequent tokens. Beyond word frequency, recent NLP research has highlighted the importance of directly considering token semantics. Lin et al. (2024) suggested that not all tokens are equally useful and proposed selective language modeling to focus on tokens consistent with the desired distribution, thus improving model performance on noisy datasets. Xiao et al. (2024) determined the visual relevance of each text token by comparing them with image inputs and assigned different loss weights accordingly. Considering our objective to prioritize positive or uncertain descriptions across various input scenarios, it is more significant to concentrate on the token semantic level rather than merely focusing on word frequency. We propose leveraging a combination of CheXbert and Integral Gradients to automatically identify key diagnostic tokens within each report and assign them higher weights, without incurring any additional computational burden during training.

Details of MIMIC-RG4

Prompts for Llama3   We meticulously design prompts to instruct the Llama3 in judging reports, focusing primarily on the following four categories of information: prior comparison, prior procedure, multi-view description and communication description, as shown in Tabel 15. In prior comparison judgement rule, we incorporate the keywords used by Nguyen et al. (2023) as a reference for Llama3 and emphasize caution with implicit comparisons. We observe that the model often overlooks the term "stable", so we highlight that it is derived from comparisons with previous reports. The prior procedure is the most challenging to assess, primarily due to the complexity of its context. Therefore, we clearly define three scenarios outlined in Table 15, including references to non-X-ray examinations, mentions of specific procedures, and the removal of specific instruments. For multi-view description and communication description, we alert Llama3 that suggestions don't fall into either category, which is frequently misclassified otherwise.

Comprehensive prompts for instructing LlaMA3 in reconstructing reports are provided in Table 16. We define reconstruction rules for common expressions, and the model is required to report any instances that fall outside these guidelines. The reconstruction rules primarily involve deleting or rewriting descriptions not inherent to the input, without introducing additional content. The sole exception is for multi-view descriptions. If multi-view descriptions are present, we add the sentence "The lateral view is recommended to assist in diagnosis" after reconstruction. The reconstruction instruction is combined with judgement instruction and judgement result to utilize LLM's chain-of-thought capability. In complex cases, a single modification may miss some expres-

Method	Prior Comparison			Prior Procedure			View			Communication		
	P	R	F1	P	R	F1	P	R	F1	P	R	F1
Keywords	90.5	**99.3**	94.7	88.9	13.8	23.9	75.0	82.5	78.6	55.8	57.1	56.5
Llama3	97.4	96.7	97.0	92.5	**84.5**	**88.1**	100.0	100.0	100.0	**97.5**	97.5	97.5
DiscBERT	**97.4**	97.4	**97.4**	93.9	79.3	86.0	**100.0**	**100.0**	**100.0**	95.9	**100.0**	**97.9**

Table 6: Comparison of various methods for quantitatively evaluating information categories in reports.

sions. Therefore, iterative modification rules are employed to facilitate multiple rounds of refinement.

Implementation Details Doctors manually label and reconstruct 200 reports as a test set, where both the finding section and the impression section are included. The 200 reconstruction samples are processed to meet the single view no longitudinal criteria, employing all four types of judgement and reconstruction prompts. As such cases encompass the other three processing types, evaluation can be conducted based on this subset alone. We choose Llama3-70B-Q4 model and deploy it on 4 RTX 3090 GPUs using Ollama. To achieve a balanced distribution of training samples for DiscBERT, we sample 11250 instances from each of the four configurations from MIMIC-CXR, totaling 45000 samples for the training set. We also select 1250 instances from each configuration, resulting in 5000 samples for the validation set. The manually annotated 200-sample test set is excluded. DiscBERT adopts a modification of the BERT-base architecture Devlin (2018) with 4 linear heads, which correspond to four categories. We utilize cross-entropy loss and Adam optimization with a learning rate of 2×10^{-5}. During training, we periodically evaluate DiscBERT on the validation set and save the checkpoint with the highest performance averaged over all 4 categories. DiscBERT is trained using a RTX 3090 GPU with a batch size of 16.

Pipeline Evaluation For DiscBERT evaluation, we compute precision (P), recall (R) and F1 score across four categories of information, as shown in Table 6. Keywords defined by Nguyen et al. (2023) are also used for comparison. We find that directly using keywords for classification poses challenges in balancing precision and recall due to linguistic ambiguity. A broader keyword selection enhances recall but reduces precision, as in the case of "prior comparison", while a narrower selection improves precision but lowers recall, as with "prior procedure". In contrast, Llama3 achieves a more balanced performance across metrics and generally surpasses keywords-based methods. DiscBERT, trained

on Llama3-generated pseudo-labels, match Llama3's performance while drastically improving inference speed, processing 200 cases in nearly 1 second compared to Llama3's 2 minutes.

For reconstruction evaluation, we compute the percentage of reports containing different category description before and after the pipeline under the setting of *sn*, using DiscBERT. We additionally calculate NLG metrics (B@2, B@4, R-L, MTR) using the LLM-reconstructed reports and manually-reconstructed reports to evaluate the similarity at the token level, as shown in Table 7. The pipeline substantially reduce uninferable information in the reports, and the carefully designed reconstruction rules also ensure a high token level similarity to manually-reconstructed reports. A qualitative result is illustrated in Figure 7.

Complete Dataset Statistics The dataset statistics for *sw*, *mn*, and *mw* are provided in Tables 8, 9, and 10. We observe two issues when directly filtering data from MIMIC-CXR based on four categories. Firstly, the data distribution is imbalanced, reflected in significant disparities in sample sizes between categories and uneven splits within categories. For instance, the *sn* category has only 16.8k training samples, and the *mn* category's test set is underrepresented. Secondly, reports within each category still contain considerable uninferable information due to the gap between the dataset and the clinical practice. After reconstruction, most categories in the MIMIC-RG4 dataset have larger sample sizes, and the splits for training, testing, and validation within each category are more balanced. Additionally, the amount of uninferable information in each category has been significantly reduced, while retaining the essential content.

Dataset	split	PC(%)	PP(%)	View(%)	Comm(%)
MIMIC CXR	Tr/84.3K	91.47	14.79	1.02	3.63
	Val/0.7K	92.84	15.81	1.49	3.38
	Ts/1.4K	93.06	16.26	1.33	7.22
MIMIC RG4	Tr/112.8K	77.36	0.28	0.20	0.00
	Val/0.9K	78.55	0.21	0.11	0.00
	Ts/2.0K	85.29	0.30	0.49	0.00

Table 8: Percentage of reports with *sw* setting, that encompass various categories of information. PC: Prior Comparison; PP: Prior Procedure; Comm: Communication; Tr: train; Ts: test.

Data	PC	PP	View	Comm	B@2	B@4	R-L	MTR
Ori.	77.0	29.0	25.0	20.0	-	-	-	-
Re.	**2.5**	**2.5**	**5.5**	**0.0**	0.755	0.688	0.692	0.480

Table 7: Reconstruction evaluation, including percentage of uninferable information and NLG metrics. PC: Prior Comparison; PP: Prior Procedure; Comm: Communication; *Ori.*: Original report; *Re.*: Reconstructed report.

Dataset	split	PC(%)	PP(%)	View(%)	Comm(%)
MIMIC CXR	Tr/42.6K	27.09	8.18	35.13	2.89
	Val/0.3K	44.73	8.26	37.31	3.36
	Ts/0.1K	74.80	31.50	42.52	13.39
MIMIC RG4	Tr/91.3K	0.26	0.14	29.22	0.04
	Val/0.7K	0.43	0.14	30.39	0.00
	Ts/1.0K	0.80	0.20	33.17	0.01

Table 9: Percentage of reports with **mn** setting, that encompass various categories of information. PC: Prior Comparison; PP: Prior Procedure; Comm: Communication; Tr: train; Ts: test.

Dataset	split	PC(%)	PP(%)	View(%)	Comm(%)
MIMIC CXR	Tr/55.1K	74.77	15.64	28.64	2.47
	Val/0.4K	72.88	14.86	27.59	3.30
	Ts/0.9K	88.34	22.48	36.69	4.56
MIMIC RG4	Tr/47.7K	67.25	0.22	27.03	0.00
	Val/0.4K	64.69	0.00	25.34	0.00
	Ts/0.8K	92.87	0.12	33.57	0.00

Table 10: Percentage of reports with **mw** setting, that encompass various categories of information. PC: Prior Comparison; PP: Prior Procedure; Comm: Communication; Tr: train; Ts: test.

Effects of ATF under Different Learnable Tokens

The number of feature tokens is crucial for multimodal large language models. Generally, a higher number of feature tokens can provide the language model with richer information, leading to improved performance. To further investigate the feature extraction and compression capabilities of the ATF module under different feature token configurations, we select various numbers of learnable tokens and evaluate their performance in comparison with the interleaved input, as shown in Table 11. In all experiments, the TLW strategy is applied with the λ value set to 1.75. We observe that with token numbers set to 64, 128, and 256, the model incorporating the ATF module demonstrate performance similar to that of interleaved input, indicating the scalability of ATF. Moreover, we find increasing the number

N_T.	ATF	CE Metrics			NLG Metrics			T
		P	R	F1	B@1	B@4	R-L	
64	✘	**0.571**	0.580	0.575	0.463	0.194	0.391	21h
	✔	0.570	**0.599**	**0.584**	**0.470**	**0.201**	**0.395**	**14h**
128	✘	0.563	0.592	0.577	0.469	0.197	0.391	25h
	✔	**0.572**	**0.599**	**0.585**	**0.472**	**0.199**	**0.393**	**17h**
256	✘	**0.573**	0.591	0.582	**0.469**	**0.200**	0.395	35h
	✔	0.572	**0.596**	**0.584**	0.465	0.199	**0.395**	**23h**

Table 11: Effects of ATF under different learnable tokens. N_T. represents the number of learnable tokens. **T** represents the training time per epoch.

of feature tokens does not yield significant improvements in this radiology report generation task.

Trend of CE with Respect to λ in TLW

To further explore how token-level loss weighting strategy influence the CE metrics, we evaluate the changes of F1 score (F1-5, F1-14) with respect to the hyperparameter λ, as shown in Figure 5 and 6. We sequentially selecte six values for λ, with the initial value corresponding to the absence of TLW strategy. The ATF module is employed in all experiments. We observe a steady increase in the model's F1 score with rising λ, which plateaus after reaching a certain threshold. Additionally, we observe that excessively high values of lambda can slightly impair the BLEU-4 score, likely due to an overemphasis on key diagnostic tokens at the expense of overall report coherence. These observations indicate that choosing an appropriate λ can effectively enhance the clinical efficacy without compromising NLG metrics. Meanwhile, this phenomenon is evident in both the first and second stages, demonstrating a positive effect across different training stages.
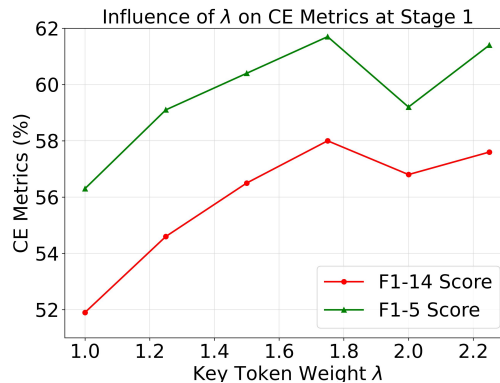

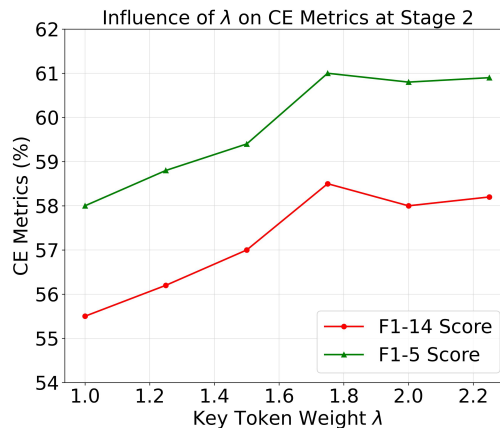
Figure 5: The influence of λ on CE metrics at stage 1.

Figure 6: The influence of λ on CE metrics at stage 2.

LLM-RG4 Hyperparameters

We set the maximum output length of Vicuna-7B v1.5 to be 150. The maximum truncation length during training is set to 100 and all reports are kept untruncated during testing. LoRA is implemented for all query and value projection matrices in the LLM, i.e., (W_q, W_v). We set rank and α in LoRA to be 32 and 64 respectively. During mixed training, we upsample *sw*, *mn*, *mw* category data to the size of *sn*. When training in the specific setting, we extend the training epochs for *sw*, *mn*, *mw* to ensure the number of iterations match or exceed that in the mixed training. Detailed hyperparameters used in inference, alignment stage and instruction stage are provided in Table 12, 13, and 14.

Hyperparameters	Values
Number of beams	3
Maximum output length	150
Minimum output length	50
Repetition penalty	2
Length penalty	2
Temperature	0

Table 12: Hyperparameters for LLM-RG4 inference.

Hyperparameters	Values
Optimizer	AdamW
Weight decay	0.01
Betas	[0.9, 0.999]
Learning rate	3×10^{-4}
Warmup rates	0.1
Number of workers	12
Type of GPU	NVIDIA A800
Number of GPU	1
Accumulate gradient batches	2
Batch size per GPU (total)	24(48)
Training precision	bfloat16
Epochs	2

Table 13: Hyperparameters for the alignment stage.

Hyperparameters	Values
Optimizer	AdamW
Weight decay	0.01
Betas	[0.9, 0.999]
Learning rate	3×10^{-4}
Warmup rates	0.1
Number of workers	12
Type of GPU	NVIDIA A800
Number of GPU	1
Accumulate gradient batches	2
Batch size per GPU (total)	16(32)
Training precision	bfloat16
Epochs	2

Table 14: Hyperparameters for the instruction-tuning stage.

Prior Comparison Judgement Rule:
System Message: Be an X-ray radiology assistant
User Message: You will be given a chest X-ray report. Please check if there are any description or mention of comparisons or references to previous xray inspections in this report. For example, expression like previous discoveries have changed, new discoveries have emerged, some things have been renoticed, some things are unchanged and treatment equipment has changed often implies a comparison. The report may include words such as new, stable, improv, resol, disappear, prior, stable, previous, again, remain, remov, similar, earlier, decreas, recurr, redemonstrate, etc. Please note that the expression of the word /stable/ is stable compared to previous reports and also belongs to the category of comparison. Please pay attention to the hidden comparisons in the expression. If it contains any comparison, please answer yes, else answer no. Just answer yes or no.
Report: ...
Judgement Result: ...

Prior Procedure Judgement Rule:
System Message: Be an X-ray radiology assistant
User Message: You will be given a chest X-ray report. Please check if the report includes one of the following three contents.
1.Please check if there is any reference to or mention of or comparison with CT or MRI or PET examination done before, rather than comparison with prior radiograph.
2.Please check if there is an explicitly description of the patient's postoperative status included, rather than guessing.
3.Please check if there is any explicitly removal of previous treatment devices such as tubes, clips, Port-A-Cath and so on, rather than implication.
If report includes any of them, please answer yes, else answer no. Just answer yes or no.
Report: ...
Judgement Result: ...

View Description Judgement Rule:
System Message: Be an X-ray radiology assistant
User Message: You will be given a chest X-ray report. Please check if it is written using a single AP or PA image as input. Specifically, please check if the report includes one of the following two contents.
1.Please check if there is any explicitly mention about what is seen in the lateral view image.
2.Please check if there is direct statement indicating that both frontal (AP or PA) and lateral view image were provided to evaluate or compare. Besides these two condition, please note that the mention of recommending lateral view to confirm does not fall under the above two condition and a descriptive term for the location does not necessarily imply that a separate lateral view image was examined. If the report meets any condition, it indicates that it was written using both frontal and lateral positions as inputs. Please answer yes, otherwise answer no. Just answer yes or no.'
Report: ...
Judgement Result: ...

Communication Description Judgement Rule:
System Message: Be an X-ray radiology assistant
User Message: You will be given a chest X-ray report. Please check if there is any mention about communication between medical professionals, such as between doctors or nurses. Please check if there is any description of transfering inspection results. Please note that suggestions are not part of communication. If is contains, please answer yes, else answer no. Just answer yes or no.
Report: ...
Judgement Result: ...

Table 15: Prompts for report judgement.

Prior Comparison Reconstruction Rule:
System Message: Be an X-ray radiology assistant
User Message: Prior Comparison Judgement Instruction + Report
Assistant Message: Judgement result
User Message: "Please rewrite the report to remove the above mentioned information while maintaining the original meaning as much as possible. Here are some rewriting principles. Please rewrite them according to the corresponding rules based on the reasons.
1. For sentences that mention comparison with a certain check, they often contain '_'. Delete the sentence that includes the comparison behavior, but retain the result;
2. For adjectives related to time, such as new and old, delete them directly. For adverbs related to time and program, such as again and so, delete them directly;
3. If there is no change, slight improvement, or deterioration in the description of previous positive symptoms that still exist, rewrite it to directly state this symptom;
4. For sentences describing a symptom that has disappeared, rewrite them as negative and mention it.
Please only give me the rewritten report, and if there is a situation where the above rules cannot be rewritten, please output: 'attention! a certain expression exceeds the current rule range.'
Rewritten Report: ...

Prior Procedure Reconstruction Rule:
System Message: Be an X-ray radiology assistant
User Message: Prior Procedure Judgement Instruction + Report
Assistant Message: Judgement result
User Message: Please rewrite the report to remove the above mentioned information while maintaining the original meaning as much as possible. Here are some rewriting principles. Please rewrite them according to the corresponding rules based on the reasons.
1. For sentences that mention the patient's postoperative state, delete the description of what postoperative state they are in;
2. For examination results obtained using other non X-ray examination methods, such as CT, MRI, PET, these examination results shall be directly deleted;
3. For sentences describing the removal of previous treatment devices such as pacemakers, clips, etc., delete them directly.
Please only give me the rewritten report, and if there is a situation where the above rules cannot be applied, please answer: 'attention! a certain expression exceeds the current rule range.'
Rewritten Report: ...

View Description Reconstruction Rule:
System Message: Be an X-ray radiology assistant
User Message: View Description Judgement Instruction + Report
Assistant Message: Judgement result
User Message: Please rewrite the report to remove the above mentioned information while maintaining the original meaning as much as possible. Here are some rewriting principles. Please rewrite them according to the corresponding rules based on the reasons.
1. For expressions provided for different views, such as AP and later views are provided, remove the expression directly while retaining the inspection results.
2. For statements that clearly state what symptoms are seen or confirmed from the lateral view, remove the statement and replace it with the statement that 'the lateral view is recommended to assist in diagnosis.'
3. For conclusions obtained from both frontal and lateral views, delete the description of the view and retain the conclusion.
Please only give me the rewritten report, and if there is a situation where the above rules cannot be applied, please answer: 'attention! a certain expression exceeds the current rule range.'
Rewritten Report: ...

Communication Description Reconstruction Rule:
System Message: Be an X-ray radiology assistant
User Message: Communication Description Judgement Instruction + Report
Assistant Message: Judgement result
User Message: Please rewrite the report to remove the above mentioned information while maintaining the original meaning as much as possible. Here are some rewriting principles. Please rewrite them according to the corresponding rules based on the reasons.
1. If a sentence describes communication with doctors and nurses, delete that sentence directly.
Please only give me the rewritten report, and if there is a situation where the above rules cannot be applied, please answer: 'attention! a certain expression exceeds the current rule range.'
Rewritten Report: ...

Iterative Modification Rules for Scenario X:
System Message: Be an X-ray radiology assistant
User Message: Judgement Instruction X + Report
Assistant Message: Judgement result 1
User Message: Reconstruction Instruction X
Assistant Message: Rewritten report 1
User Message: Judgement Instruction X + Rewritten Report 1
Assistant Message: Judgement result 2
User Message: Reconstruction Instruction X
Rewritten Report2: ...
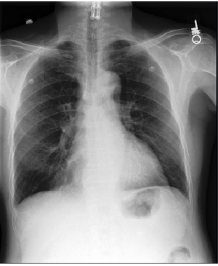
Table 16: Prompts for report reconstruction.

Original report: *Finding : pa and lateral radiographs of the chest were acquired . there is a 5-mm nodular opacity in right mid lung projecting over the posterior rib possibly a lung nodule . ill-defined opacity at the right medial lung base with associated silhouetting of the lower right heart border is not significantly changed compared to prior radiographs from and is likely related to a prominent epicardial fat pad as seen on ct from . no focal consolidations are seen . there is evidence of mild emphysema . there are no pleural effusions . no pneumothorax is seen . the cardiac and mediastinal contours are normal . cervical fusion hardware is not fully assessed . multilevel degenerative changes of the thoracic spine are noted as before impression : no acute cardiac or pulmonary process . possible 5-mm right mid lung nodule should be further evaluated with chest ct . findings and recommendation were discussed with dr . by dr . at 5 :15 pm . via telephone on the day of the study .*

Reconstructed sn: *Finding: pa and lateral radiographs of the chest were acquired . There is a 5-mm nodular opacity in right mid lung projecting over the posterior rib , a lung nodule . There is an ill-defined opacity at the right medial lung base with associated silhouetting of the lower right heart border is not significantly changed compared to prior radiographs from . is likely related to a prominent epicardial fat pad as seen on ct from No focal consolidations are seen. There is evidence of emphysema. There are no pleural effusions. No pneumothorax is seen. The cardiac and mediastinal contours are normal. cervical fusion hardware is not fully assessed . Multilevel degenerative changes of the thoracic spine are noted as before. Impression: No acute cardiac or pulmonary process. A 5-mm right mid lung nodule should be further evaluated. findings and recommendation were discussed with dr . by dr . at 5 :15 pm . via telephone on the day of the study .*

Reconstructed mn: *Finding: PA and lateral radiographs of the chest were acquired. There is a 5-mm nodular opacity in right mid lung projecting over the posterior rib, a lung nodule. There is an ill-defined opacity at the right medial lung base with associated silhouetting of the lower right heart border. is not significantly changed And is likely related to a prominent No focal consolidations are seen. There is evidence of emphysema. There are no pleural effusions. No pneumothorax is seen. The cardiac and mediastinal contours are normal. cervical fusion hardware is not fully assessed . Multilevel degenerative changes of the thoracic spine are noted as before. Impression: No acute cardiac or pulmonary process. A 5-mm right mid lung nodule should be further evaluated. findings and recommendation were discussed with dr . by dr . at 5 :15 pm . via telephone on the day of the study .*

Reconstructed sw: *Finding: PA and lateral radiographs of the chest were acquired. There is a 5-mm nodular opacity in right mid lung projecting over the posterior rib, possibly a lung nodule. Ill-defined opacity at the right medial lung base with associated silhouetting of the lower right heart border is not significantly changed And is likely related to a prominent epicardial fat pad as seen on ct from . . No focal consolidations are seen. There is evidence of mild emphysema. There are no pleural effusions. No pneumothorax is seen. The cardiac and mediastinal contours are normal. cervical fusion hardware is not fully assessed . Multilevel degenerative changes of the thoracic spine are noted. Impression: No acute cardiac or pulmonary process. Possible 5-mm right mid lung nodule should be further evaluated. A lateral view is recommended to assist in diagnosis. findings and recommendation were discussed with dr . by dr . at 5 :15 pm . via telephone on the day of the study .*

Reconstructed mw: *Finding: PA and lateral radiographs of the chest were acquired. There is a 5-mm nodular opacity in right mid lung projecting over the posterior rib, possibly a lung nodule. Ill-defined opacity at the right medial lung base with associated silhouetting of the lower right heart border is not significantly changed And is likely related to a prominent epicardial fat pad as seen on ct from . No focal consolidations are seen. There is evidence of mild emphysema. There are no pleural effusions. No pneumothorax is seen. The cardiac and mediastinal contours are normal. cervical fusion hardware is not fully assessed . Multilevel degenerative changes of the thoracic spine are noted. Impression: No acute cardiac or pulmonary process. Possible 5-mm right mid lung nodule should be further evaluated. findings and recommendation were discussed with dr . by dr . at 5 :15 pm . via telephone on the day of the study .*

Figure 7: A qualitative illustration of the reconstructed reports. We use strikethrough to indicate the differences between the original reports and reconstructed reports. Different category descriptions are highlighted using the same color, red: prior comparison; orange: prior procedure; blue: view description; green: communication. The reconstructed reports show close alignment with the input while minimizing information loss.